Reconnection and small-scale fields in 2D-3V hybrid-kinetic driven turbulence simulations

2017 New J. Phys. 19 025007

(http://iopscience.iop.org/1367-2630/19/2/025007)

New Journal of Physics
The open access journal at the forefront of physics

Deutsche Physikalische Gesellschaft DPG
IOP Institute of Physics

Published in partnership with: Deutsche Physikalische Gesellschaft and the Institute of Physics

OPEN ACCESS

RECEIVED
29 September 2016

REVISED
25 January 2017

ACCEPTED FOR PUBLICATION
26 January 2017

PUBLISHED
21 February 2017

PAPER

Reconnection and small-scale fields in 2D-3V hybrid-kinetic driven turbulence simulations

S S Cerri[1] **and F Califano**

Physics Department 'E. Fermi', University of Pisa, Largo B. Pontecorvo 3, I-56127 Pisa, Italy
[1] Author to whom any correspondence should be addressed.

E-mail: silvio.cerri@df.unipi.it **and** francesco.califano@unipi.it

Keywords: plasma turbulence, space plasmas, magnetic reconnection, Vlasov simulations

Abstract

The understanding of the fundamental properties of turbulence in collisionless plasmas, such as the solar wind, is a frontier problem in plasma physics. In particular, the occurrence of magnetic reconnection in turbulent plasmas and its interplay with a fully-developed turbulent state is still a matter of great debate. Here we investigate the properties of small-scale electromagnetic fluctuations and the role of fast magnetic reconnection in the development of a quasi-steady turbulent state by means of 2D-3V high-resolution Vlasov–Maxwell simulations. At the largest scales turbulence is fed by external random forcing. We show that large-scale turbulent motions establish a $-5/3$ spectrum at $k_\perp d_i < 1$ and, at the same time, feed the formation of current sheets where magnetic reconnection occurs. As a result coherent magnetic structures are generated which, together with the rise of the associated small-scale non-ideal electric field, mediate the transition between the inertial and the subproton-scale spectrum. A mechanism that boosts the magnetic reconnection process is identified, making the generation of coherent structures rapid enough to be competitive with wave mode interactions and leading to the formation of a fully-developed turbulent spectrum across the so-called ion break.

1. Introduction

Space plasmas are probably the best laboratory for the study of collisionless plasma turbulence, as the Earth's environment has become accessible to increasingly accurate direct measurements [1]. *In situ* observations in the solar wind and in the terrestrial magnetosheath have provided the possibility of obtaining relevant constraints on the turbulent energy spectra, determining the typical values for their slopes and, in particular, revealing the presence of a break in the electromagnetic fluctuations cascade around the ion kinetic scale [2–7]. Such break separates the so-called 'inertial range' spectrum, developing at the MHD scales, from the kinetic spectrum that arises at scales smaller than the ion gyroradius (also referred to as the 'dissipation' or 'dispersion' range spectrum). Such a transition is clear evidence of a change in the physics underlying the cascade process, and its understanding in terms of kinetic physics is today a matter of a strong debate. One of the main properties allowing one to distinguish between the inertial range and the dispersion range spectrum is that the former is composed of broadband fluctuations of quasi-2D Alfvénic fluctuations [2, 7–9]. The ion kinetic spectrum instead can be seen as a mixture of different contributions, such as wave-like fluctuations (kinetic Alfvén waves (KAW), whistler waves, Alfvén ion cyclotron (AIC)), or coherent (magnetic) structures, as, e.g., Alfvén vortices and structures resulting from the destabilization of ion-scale current sheets, which also contribute to the spectrum properties (see [10] and references therein).

From a theoretical point of view possible explanations for the observed spectra are given in terms of nonlinear normal mode interactions such as, for instance, the development of a kinetic Alfvén wave cascade [11–15] and/or a whistler cascade [15, 16], while the possible role of ion Bernstein waves is still unclear [11]. In this context, the presence of relatively large-amplitude fluctuations and the contribution of coherent structures to the turbulent cascade make the picture even more complicated and its interpretation in terms of

only linear modes still under debate [17]. An important role can be played by coherent structures, as they represent a different path (with respect to wave modes) to contribute to the turbulent cascade around and below the ion kinetic scales in order to allow and/or speed up the nonlinear transfer of the electromagnetic fluctuations beyond the inertial spectrum. Despite these processes, that come into play well before collisional effects, are not yet well understood, their importance in partially 'replacing' the role of collisional dissipation in plasma turbulence is now widely accepted [18, 19]. At the same time the dynamics of these coherent structures may provide some additional self-consistent energy injection [20–22] and thus supporting the continuation of the cascade across and below ion kinetic scales. In this scenario, the non-ideal electric field acts as a mediator and its development at the kinetic scales marks the transition to a state in which current sheets are continuously formed by large-scale turbulent motions and destroyed by small-scale reconnection. The interplay and balance of these effects brings the system towards a self-regulated fully-developed turbulent state.

In order to investigate such complex dynamics, several analytical [11–16, 23, 24] and numerical [25–41] studies have been presented over the last few years. So far numerical studies have been performed mainly within a decaying turbulence framework, while a continuous forcing mechanism permits reaching a 'quasi-steady turbulent regime' over which the statistics of the performed analysis can be improved. There exist a few recent works on continuously driven kinetic turbulence, characterized by driving a specific wave mode [30, 31, 38] or by injecting purely incompressible fluctuations [28, 29]. Here we intend to relax these conditions on the external forcing by injecting random, partially compressible large-scale momentum fluctuations in the system. Vlasov–Eulerian simulations [42, 43] are well suited for the study of the turbulent cascade properties at kinetic scales because of the very low noise of the numerical scheme. However, a Eulerian approach to the Vlasov equation (hereafter Vlasov simulations) is technically challenging because of the enormous computational requirements, especially in high-dimensional phase space. A full 3D-3V (three dimensions in real space and three dimensions in velocity space) Vlasov simulation, from large MHD scales down to sub-Larmor scales, is beyond today's computational capabilities. For these reasons, even if solar wind plasma turbulence is an intrinsically 3D problem, Vlasov simulations are still mainly performed in a reduced 2D-3V phase space able to shed light on many important aspects of turbulent dynamics, especially in the presence of a quite strong background magnetic field. In fact, the intrinsic anisotropy of the MHD turbulent cascade and the strong damping of parallel modes [11, 12, 47, 48] favor the development of strong nonlinear turbulent interactions mainly in the plane perpendicular to the background magnetic field. Therefore we are convinced that '2.5D' simulations do retain several very important dynamical features underlying the fully 3D dynamics [34, 44–46].

In this paper we focus on the problem of collisionless plasma turbulence across the ion kinetic scales, from the end of the MHD turbulent cascade down to well below the ion gyroradius and/or inertial length. Our study is based on numerical simulations of continuously driven turbulence within a hybrid Vlasov–Maxwell (HVM) model of plasma, in a reduced 2D-3V phase space. First results concerning the observed turbulent spectra and their interpretation as a function of the plasma beta parameter have been recently reported [41]. Here instead we focus our attention on the mechanisms underlying the generation of a fully-developed stationary turbulent state in a $\beta = 1$ plasma, first by addressing the problem of the role of small-scale electromagnetic fields and of the formation of coherent structures via fast magnetic reconnection.

The paper is organized as follows: in section 2 the governing equations adopted in our plasma model are described, along with the initial simulation conditions and plasma parameters (section 2.1). In section 3 the results of direct numerical integration of our model equations are presented and discussed. In particular, our analysis will focus on the role of current sheets and small-scale non-ideal electric field on the development of turbulence (section 3.1) and on the reconnection processes taking place in a turbulent environment (section 3.2). Finally, conclusions are given in section 4.

2. HVM

The Vlasov–Maxwell system of equations is solved in phase space using the so-called hybrid approximation where ions are fully kinetic and electrons are assumed as a neutralizing massless fluid [43]. In the following, all equations are normalized to the ion mass m_i, the ion cyclotron frequency Ω_{ci}, the Alfvén velocity v_A and to the ion skin depth $d_i = v_A/\Omega_{ci}$. Furthermore, we add an external random forcing term of very low amplitude in the ion Vlasov equation in order to feed the turbulence on the largest wavelengths of the system. The forcing is a random, space-dependent forcing δ-correlated in time. It injects momentum into the system with a prescribed average power density ϵ and it is composed of an incompressible and a compressible component (see section 2.1).

The HVM system of equations in dimensionless units is given by the Vlasov equation for the ion distribution function (hereafter DF) $f_i = f_i(\mathbf{x}, \mathbf{v}, t)$,

$$\frac{\partial f_i}{\partial t} + \mathbf{v} \cdot \frac{\partial f_i}{\partial \mathbf{x}} + (\mathbf{E} + \mathbf{v} \times \mathbf{B} + \mathbf{F}_{\rm ext}) \cdot \frac{\partial f_i}{\partial \mathbf{v}} = 0, \tag{1}$$

where $\mathbf{F}_{\rm ext}$ is the forcing term, and by the Faraday's (Ampére's) equation,

$$\frac{\partial \mathbf{B}}{\partial t} = -\nabla \times \mathbf{E}, \quad \nabla \times \mathbf{B} = \mathbf{J} \tag{2}$$

where the displacement current term has been neglected. Finally, the generalized Ohm's law for the electron response reads,

$$\mathbf{E} = -\mathbf{u} \times \mathbf{B} + (\mathbf{J} \times \mathbf{B})/n - \nabla \mathbf{P}_e/n \tag{3}$$

where electron inertia has been neglected and we assumed quasi-neutrality $n_i \simeq n_e = n$. The number density n and the ion mean velocity $\mathbf{u}$ are computed as velocity-space moments of the ions DF. We assume an isothermal equation of state for the electron pressure, $P_e = nT_{0e}$, with a given initial electron-to-ion temperature ratio T_{0e}/T_{0i}.

The set of equations (1)–(3) is solved in a 2D-3V phase space in slab geometry using an Eulerian algorithm [42] which combines the so-called splitting scheme with the current advanced method [43]. All vector fields are fully three-dimensional, for instance $\mathbf{B} = B_x(x, y)\mathbf{e}_x + B_y(x, y)\mathbf{e}_y + B_z(x, y)\mathbf{e}_z$, a configuration usually referred to as '2.5D'. In order to avoid spurious numerical effects at very small scales, we adopt spectral filters that act only on the high-k part of the spectrum. Furthermore, additional numerical diffusivity at very small scales in phase space is intrinsically included in the Eulerian algorithm which integrate the ions' DF [42].

2.1. Simulation setup

We initialize our simulations by an ion-Maxwellian thermal plasma,

$$f_i(x, y, v_x, v_y, v_z; t = 0) = \frac{n_0}{(2\pi v_{{\rm th},i}^2)^{3/2}} e^{-(v_x^2+v_y^2+v_z^2)/(2\, v_{{\rm th},i}^2)}, \tag{4}$$

where $n_0 = 1$ is the initial (constant) plasma density. In the following we consider the case of a unity ion plasma beta, $\beta_i = 1$, with a corresponding thermal velocity (in Alfvén speed units) $v_{{\rm th},i} = \sqrt{\beta_i/2}$ and an isotropic temperature $T_{0i} = T_{0e} = 0.5$ at $t = 0$. The initial magnetic field is given by a constant background field perpendicular to the simulation plane, $B_0\mathbf{e}_z$, where $B_0 = 1$, with a superimposed small-amplitude 3D perturbation, $\delta\mathbf{b} = \delta b_x\mathbf{e}_x + \delta b_y\mathbf{e}_y + \delta b_z\mathbf{e}_z$, computed as the curl of a vector potential, $\delta\mathbf{b} \equiv \nabla \times \delta\mathbf{A}$. The initial magnetic perturbations have a relatively small amplitude, $\delta b/B_0 \sim 0.01$, and are distributed over the very large-scale part of the spectrum, $0.1 \leqslant (k_\perp d_i)_{\delta b} \leqslant 0.3$.

The system is driven to a quasi-steady turbulent state via an external random force, $\mathbf{F}_{\rm ext}(\mathbf{x}, t)$, δ-correlated in time and injecting momentum with a prescribed average power density ε. The external forcing is computed in Fourier space with a corresponding correlation tensor given by

$$\langle F_{\mathbf{k},i}(t) F^*_{\mathbf{k},j}(t') \rangle = \chi(k) \left[\alpha_1 \left(1 - \frac{k_i k_j}{|\mathbf{k}|^2} \right) + \alpha_2 \left(\frac{k_i k_j}{|\mathbf{k}|^2} \right) \right] \delta(t - t'), \tag{5}$$

where $\langle ... \rangle$ denote ensemble (spatial) averaging, $\mathbf{k}$ is the prescribed wave vector and $\chi(k)$ is a scalar function that depends only on the modulus of $\mathbf{k}$. The coefficients α_1 and α_2 quantify the degree of incompressibility and compressibility, respectively. In the present simulations, the external forcing continuously injects the same amount of incompressible and compressible fluctuations, $\alpha_1 = \alpha_2 = 1/2$, into the two largest wave numbers allowed by the simulation box, $0.1 \leqslant (k_\perp d_i)_{\rm Fext} \leqslant 0.2$, with an average power density $\epsilon = 5 \times 10^{-4}$ [41].

The 5D phase space domain (x, y, v_x, v_y, v_z) has been chosen to have the following dimensions. The physical domain is a squared box with length $L = 20\pi d_i$, and we use $N_x = N_y = 1024$ uniformly distributed grid points. Periodic boundary conditions are imposed in both the x and y-direction. The velocity domain range is limited by $v_{{\rm max},x} = v_{{\rm max},y} = v_{{\rm max},z} = \pm 5$ (in $v_{{\rm th},i}$ units), using $N_{vx} = N_{vy} = N_{vz} = 51$ uniformly distributed grid points. At the boundaries of the velocity domain, the DF is forced to be zero.

3. Simulation results

In the following we focus on the role of the formation of coherent magnetic structures in a continuously forced turbulent environment, and on their possible feedback on the turbulence itself. Such structures are preceded by the formation of several intense elongated current sheets (hereafter CSs) with a characteristic width of the order of the ion scale length, d_i and/or ϱ_i (see [52] and references therein). As discussed in the Introduction (section 1), CSs and other type of magnetic coherent structures are today routinely observed by satellite measurements [18, 53]. It has been suggested that they significantly contribute to the magnetic fluctuation spectrum around ion scales [10]. In our simulations we observe that the CSs, once formed, are then disrupted on a characteristic timescale of the order of a few tens of ion times via fast magnetic reconnection, leading to the

formation of several island-like coherent structures and allowing the system to rapidly reach a fully-developed turbulent state. We identify a fully-developed (or quasi-steady) turbulent state with that phase characterized by the stationarity of the energy spectra. In this context, the role of the CSs disruption mechanism leading to the formation of coherent structures such as the magnetic islands, and the role of the small-scale electric field is crucial. Note that other different kind of structures as, for instance Alfvén vortex-like structures [49], could be generated even if we cannot clearly identify them here because of the strictly 2D dynamics imposed by our model. We finally underline the importance of the feedback between the turbulent cascade and magnetic reconnection. Indeed, on one side reconnection is crucial to let the energy cascading from the inertial spectrum to access, or at least to fasten the access, to the subproton ion-scale spectrum. Such process is eventually responsible for the transition to a fully-developed turbulent state. On the other hand, turbulent motions are able to provide for the continuous generation of new CSs where fast reconnection again occurs as observed, for instance, in numerical simulations even using a fluid approach [50].

3.1. Transition to fully-developed turbulence and the role of small-scale fields

In the initial phase of the simulation the system develops large-scale motions dominated mainly by a MHD dynamics, as outlined by nearly superposition of the density and parallel magnetic fluctuations, δn and $\delta b_{\parallel}$. Here parallel (and perpendicular) is defined with respect to the direction of the initial background magnetic field, $B_0\mathbf{e}_z$. The external forcing continuously injects momentum in the system. Correspondingly, the average kinetic and magnetic energies, $\langle n|\mathbf{u}_i|^2\rangle$ and $\langle|\mathbf{B}|^2\rangle$, grow more or less linearly in time during an initial phase, up to a saturation stage after which the system reaches a quasi-steady turbulent state. On the other hand, the average out-of-plane squared current density, $\langle J_z^2\rangle$, grows exponentially in time before saturation, showing CSs formation as a fast and fundamental process in plasma turbulence in agreement with MHD simulations (see, e.g., [51] and references therein). The saturated phase is reached after a characteristic time of about 150 ion cyclotron times, whereas a proper 'stationary' fully-developed turbulent state is achieved starting roughly from about $t\Omega_{ci} \sim 200$, after which the turbulent energy spectra, on average, do not vary anymore. In terms of the outer-scale nonlinear time estimated from a Kolmogorov-like argument, $\tau_{\rm nl}(L) \sim L^{2/3}/\epsilon^{1/3}$, saturation is reached after a few $\tau_{\rm nl}$.

For the given forcing amplitude $\epsilon = 5 \times 10^{-4}$, the perpendicular ion velocity fluctuations $u_{i,\perp} = [u_{i,x}^2 + u_{i,y}^2]^{1/2}$ in the fully-developed turbulent state vary mainly in the range $0.01 \lesssim u_{i,\perp} \lesssim 0.6$ reaching locally (and for a limited time duration) peak values of the order of $u_{i,\perp}^{\rm max} \simeq 0.9$. The rms value of $u_{i,\perp}$, averaged over a time interval of about $\Delta t\Omega_{ci} \sim 100$ after the initial growth phase, turns out to be $\overline{u_{i,\perp}^{\rm rms}} \sim 0.3$ (in our notation the bar stands for time average, whereas the $\langle ...\rangle$ represents space average). Correspondingly, the system develops in-plane magnetic fluctuations that vary in the range $0.01 \lesssim \delta b_{\perp} \lesssim 0.3$, but with local peaks reaching values up to $\delta b_{\perp} \simeq 0.6$ which are however very shortly-lived phenomena (order of very few ion cyclotron times). The rms value of the in-plane magnetic fluctuations, time averaged over the fully-developed turbulent state, turns out to reach ~10% of the background field, $\overline{\delta b_{\perp}^{\rm rms}} \sim 0.1$. The resulting Alfvén ratio (i.e., the ratio between the kinetic and the magnetic energies) turns out to be of about $r_A \sim 9$, whereas SW measurements point to a ratio of order unity in the MHD range. However such a large value of $r_{\rm A}$ is limited to the first two modes, $k_{\perp} d_i = 0.1$ and 0.2, and it is a direct consequence of the external drive that continuously injects momentum at those scales. Immediately after the Alfvén ratio self-consistently sets to $r_A \sim 1$ and stays throughout the rest of the MHD inertial range, $0.3 \leqslant k_{\perp} d_i \leqslant 1$. Therefore, such a feature do not affect the interpretation of the results in terms of SW turbulence.

The formation of many CSs is a common feature of all simulations performed, regardless of the value of the plasma beta, of the injected energy, of the nature of $\mathbf{F}$ (partially compressible or purely incompressible), and/or of the resistivity (but assuming $S \gtrsim 10^3$). Such CSs are thin, elongated structures of typical length of the order of tens of d_i with corresponding strong magnetic shear of typical scale length of the order of d_i, randomly located in the simulation plane (see, e.g. figure 1, left column). CSs formation and its consequences can be seen as a general feature of plasma turbulence, as observed in the past starting from the early MHD up to the very recent kinetic simulations [39, 45, 51, 52], and recently outlined also by satellite observations [18, 19, 54]. The typical timescale for the formation of the first wider CSs is of the order of few tens of ion times, while they shrink to d_i-scale width on nearly 100 ion times. Such timescale is in agreement with the corresponding typical eddy-turnover time of the large-scale motions, $\tau_L \sim L/u_{\perp}$.

In figure 1 we show the shaded iso-contours of the out-of-plane current density J_z (left column), and of the electric and magnetic energy spectra (right column) at $t = 120, 170, 228$ (top to bottom, respectively). The first column highlights the basic steps of the simulation: CSs generation, their width shrinking, their disruption via reconnection instabilities and the generation of many ion-scale coherent structures as well as small-scale fluctuations. The second column shows the formation of the inertial spectrum, the following rise of the subproton range energy spectrum and the emergence of the ion break as a consequence of CSs disruption.

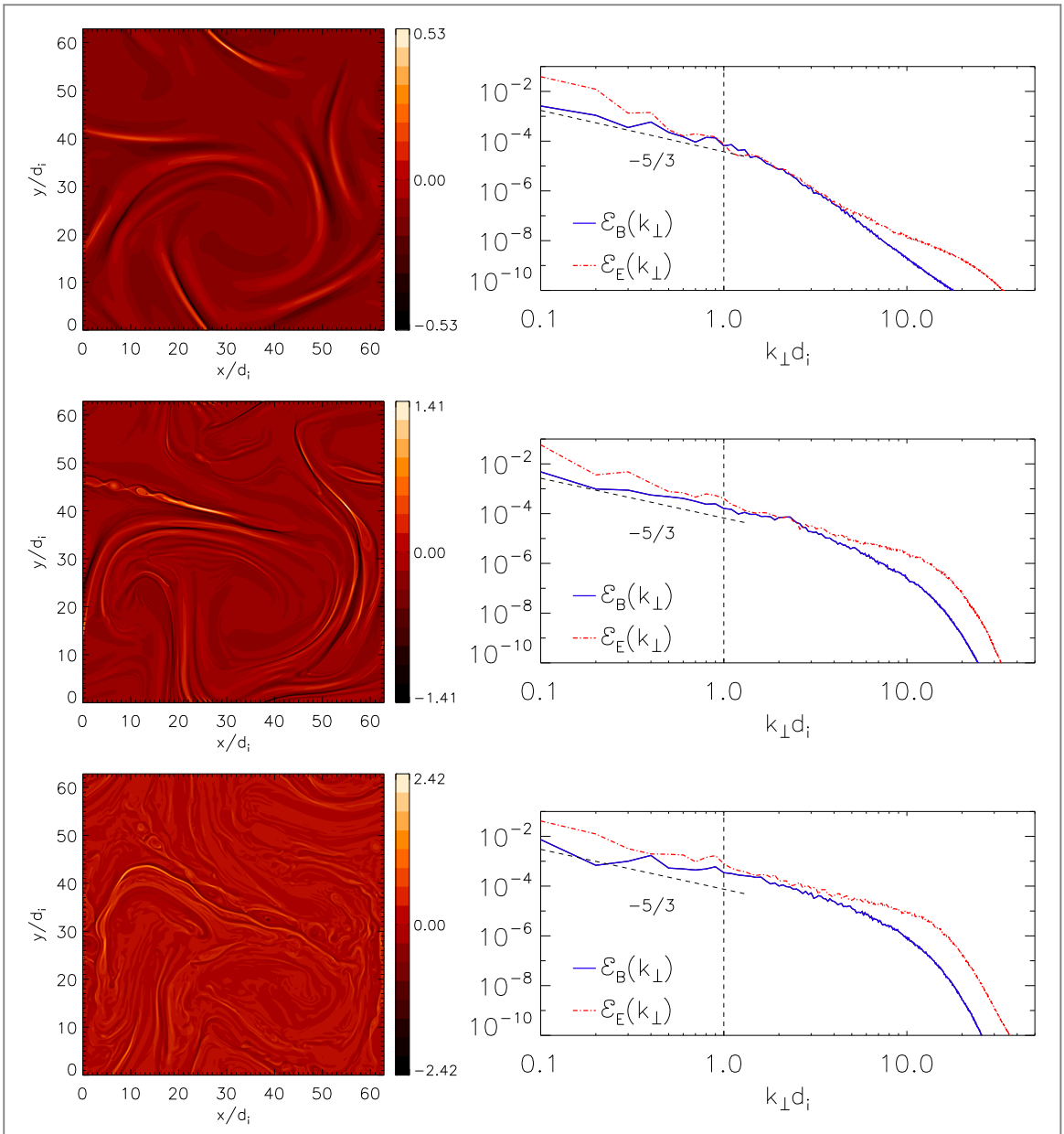

Figure 1. Out-of-plane current density, j_z (left column), and electric and magnetic energy spectra, $E_E(k_\perp)$ and $E_B(k_\perp)$ (right column), at $t = 120$, 170, and 228 (top to bottom, respectively). A $k_\perp^{-5/3}$ slope is given as a reference (dashed straight line).

CSs disruption and the corresponding formation of several magnetic coherent structures is the turning point of our simulation for what concerns the transition to a fully-developed turbulent state, as shown by the last frames of figure 1. Indeed, the CSs narrowing process and their destabilization via magnetic reconnection is intimately related with the growth of small-scale electric and magnetic fluctuations that eventually bring the system to the achievement of the quasi-steady turbulent state. By looking at the large-scale fluctuations component of the spectrum (see figure 1, right frames), we see that a $-5/3$ power law has been already established at $t\Omega_{ci} = 120$, when the system is still far from a fully-developed turbulent state, and it is maintained until the end of the simulation. Only when reconnection processes start and take over, we observe a significant rise of small-scale electromagnetic fluctuations and, eventually, the transition to turbulence. In other words the development of a $k_\perp d_i > 1$ spectrum is related to the triggering of many fast magnetic reconnection events that quickly push the system into a fully turbulent state. The spectra plotted in figure 1 are not time averaged and therefore far from being smooth, especially at $k_\perp d_i < 1$. Furthermore, at $k_\perp d_i \leqslant 0.2$ parallel magnetic fluctuations driven by the external, partially compressible forcing have a larger amplitude with respect to their perpendicular counterpart; these two quantities become then immediately of the same order in the inertial part of the spectrum, $0.3 \leqslant k_\perp d_i \leqslant 1$.

Let us consider the electric field fluctuations computed by using the generalized Ohm's law in equation (3). The total electric field is made by an ideal (MHD) contribution, $\mathbf{E}_{\rm MHD} \equiv -\mathbf{u}_i \times \mathbf{B}$, and by two non-ideal

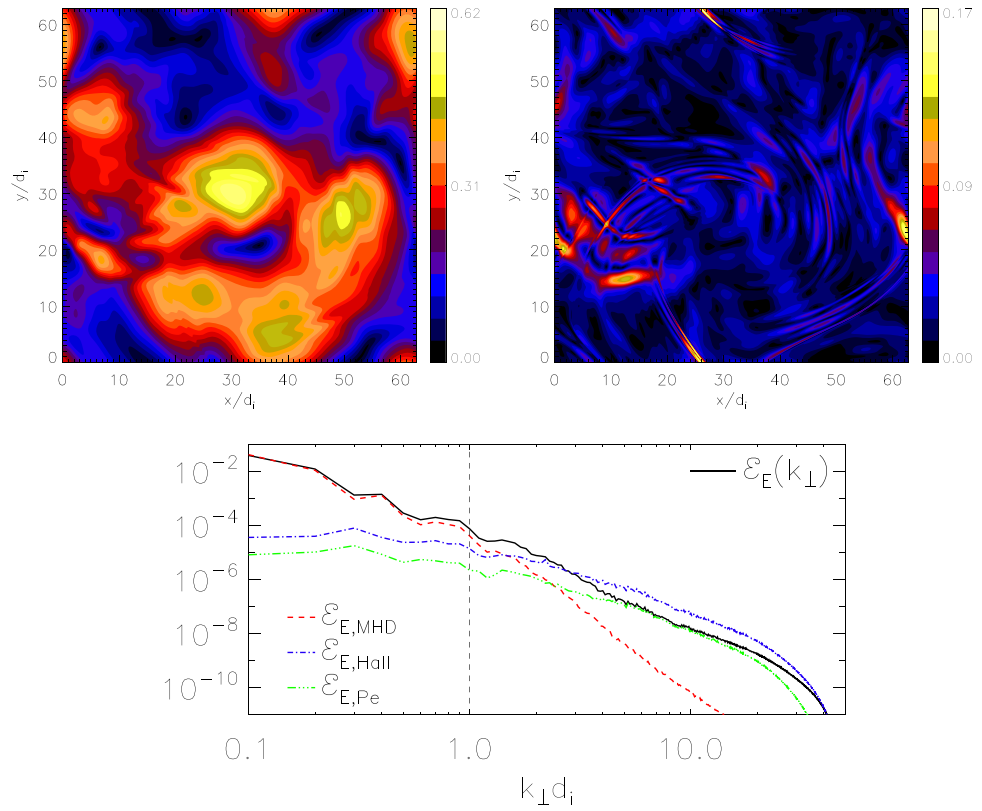

Figure 2. Time $t\Omega_{ci} = 120$. Top panels: shaded iso-contours of the modulus of the in-plane ideal electric field, $E_{\mathrm{MHD},\perp}$, left, and of the Hall component, $E_{\mathrm{H},\perp}$, right. Bottom: spectrum of the ideal electric field (red, dashed), of the Hall term (blue, dashed-dotted) and of the electron pressure gradient term (green, dashed-triple-dotted), compared to the total electric energy spectrum (black, continuous).

contributions, the Hall electric field, $\mathbf{E}_{\mathrm{H}} \equiv \mathbf{J} \times \mathbf{B}/n$, and the electron pressure gradient term, $\mathbf{E}_{P_e} \equiv -\nabla P_e/n$. By directly addressing both spectral properties [39] and real space behavior of these components, and their change with time, we can relate these aspects to the transition shown in figure 1, highlighting the link between fast magnetic reconnection and fully-developed turbulence. In figures 2 and 3 we show at $t\Omega_{ci} = 120,\ 228$ the in-plane modulus of the ideal electric field component, $E_{\mathrm{MHD},\perp}$, the Hall component of the electric field, $E_{\mathrm{H},\perp}$ and the energy spectra of the different electric field terms. As expected, at $k_\perp d_i < 1$ the leading contribution to the electric field spectrum is given by the ideal component, $\mathbf{E}_{\mathrm{MHD}}$, whereas the non-ideal terms represent the dominant contribution at $k_\perp d_i > 1$. The ideal contribution at large scales, $k_\perp d_i < 1$, does not change significantly when the system goes through the transition from the end of the 'saturated' phase to the fully-developed turbulent state (see figures 2–3, bottom panels), as shown also by the vortical-like pattern in real space of $\mathbf{E}_{\mathrm{MHD}}$ in the top left panels of figures 2–3. Indeed after the transition we observe just an enrichment of the meso- and small-scale fluctuations since a significant change takes place only at $k_\perp d_i \gtrsim 1$. Such large-scale vortical pattern of the ideal electric field is driven by the in-plane injection of velocity fluctuations,

$$\delta\mathbf{E}_{\mathrm{MHD}} \approx -\delta\mathbf{u}_i \times \langle\mathbf{B}\rangle \sim B_0\, \delta u_\perp \mathbf{e}_\perp, \tag{6}$$

where we have neglected second-order contributions. The energy spectrum of the MHD electric field at $k_\perp d_i < 1$ is thus given by $\mathbf{E}_{\mathrm{MHD},\perp}$ and it is proportional to the spectrum of $\mathbf{u}_\perp$, $\mathcal{E}_{\mathrm{MHD}}(k_\perp) \sim \mathcal{E}_{u\perp}(k_\perp)$. Such superposition of the two spectra is observed at low wave numbers (not shown here).

On the other hand, the non-ideal electric field behavior strongly changes when passing from the saturated phase to the fully-developed turbulent regime. Correspondingly, the subproton electric energy spectrum changes triggered by the dynamics induced by fast reconnection. In fact, let us consider the Hall electric field, whose fluctuations are given by

$$\begin{aligned}\delta\mathbf{E}_{\mathrm{H}} &\simeq \frac{\delta\mathbf{J}\times\langle\mathbf{B}\rangle}{\langle n\rangle} + \frac{\langle\mathbf{J}\rangle\times\delta\mathbf{b}}{\langle n\rangle} - \frac{\langle\mathbf{J}\rangle\times\langle\mathbf{B}\rangle}{\langle n\rangle}\frac{\delta n}{\langle n\rangle} \\ &\sim \frac{B_0}{n_0}k_\perp\left[(2+\beta)\delta B_\parallel + \frac{k_\parallel}{k_\perp}\delta B_\perp\right]\mathbf{e}_\perp,\end{aligned} \tag{7}$$

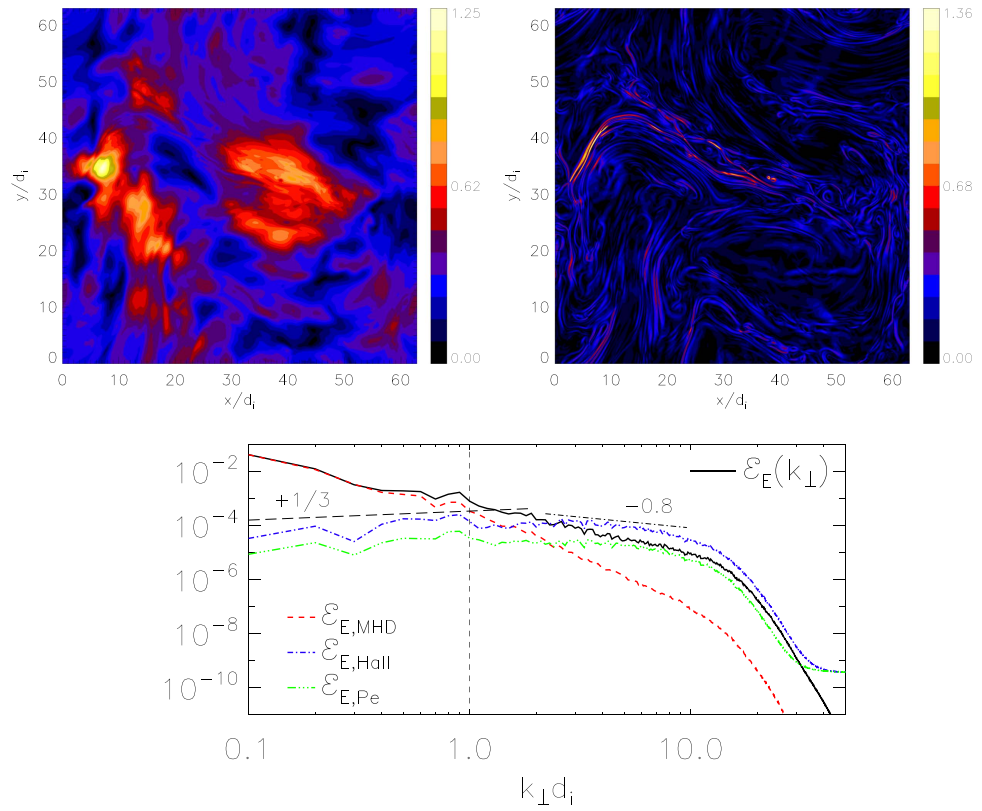

Figure 3. Same as figure 2, at time $t\Omega_{ci} = 228$. Slopes are given as references.

where second-order terms have been neglected and we have made use of $\delta\mathbf{J} = \nabla \times \delta\mathbf{b}$. Due to the 2.5D configuration, the term $k_\parallel/k_\perp \ll 1$ can also be neglected, even if a non-zero $k_\parallel \equiv \mathbf{k}\cdot\mathbf{b}$ can locally arise and be relevant for the cascade even in 2.5D [41]. The leading contribution to $\mathbf{E}_\mathrm{H}$ is therefore given by its perpendicular component, whose energy spectrum is $\mathcal{E}_{\mathrm{H},\perp} \propto k_\perp^2 \mathcal{E}_{B\parallel}$. The parallel component of $\mathbf{E}_\mathrm{H}$ is a second-order quantity in the fluctuations, $\delta E_{\mathrm{H},\parallel} \propto k_\perp \delta B_\parallel \delta B_\perp$, and its spectrum is given by $\mathcal{E}_{\mathrm{H},\parallel} \propto k_\perp^3 \mathcal{E}_{B\perp}\mathcal{E}_{B\parallel}$. The same holds for $E_{Pe,\perp}$ and for its energy spectrum, related to the magnetic spectrum as $\mathcal{E}_{Pe}(k_\perp) \propto k_\perp^2 \mathcal{E}_{B\parallel}(k_\perp)$ assuming $\mathcal{E}_n(k_\perp) \sim \mathcal{E}_{B\parallel}(k_\perp)$, as expected for KAW-like fluctuations (see [41] and references therein). The parallel magnetic fluctuations follow nearly a $k_\perp^{-5/3}$ power law at $k_\perp d_i \lesssim 1$ and, as soon as a quasi-steady turbulent state is reached, it steepens to nearly $k_\perp^{-2.8}$ at small scales (not shown here). This corresponds to a change in the slopes of $\mathcal{E}_\mathrm{H}$ and $\mathcal{E}_{Pe}$, from $+1/3$ to about -0.8, as shown in figure 3 (bottom panel). Another signature of the slope variation of the non-ideal electric field spectrum around $k_\perp d_i \sim 2$ is visible on the iso-contours of $E_{\mathrm{H},\perp}$ (see figure 3, top right frame) showing the small-scale pattern formation after reconnection develops. The same holds for the iso-contours of $E_{Pe,\perp}$ (not shown here).

Generally speaking, the non-ideal electric fluctuations move through from being dominated by the small-scale gradients at the front of the large-scale vortical motions (figure 2, upper panels), to being localized within CSs, at the borders of island-like magnetic structures and at the reconnection sites (whose typical sizes are of the order of $\sim d_i$), as soon as fast turbulent reconnection begins (figure 3, upper panels). This relates the fast reconnection processes to the sudden change of the spectral slopes of the small-scale electromagnetic energy spectra that rapidly evolve into the quasi-steady slopes observed during the fully-developed turbulent phase, both in time and space (with a break at scale $\sim d_i$). As the first significant fast reconnection events take place at about $t\Omega_{ci} = 170$, a small bump and a sharp break emerge in the magnetic spectrum at $k_\perp d_i \sim 2$ (figure 1, mid right panel). This spectral feature also marks the transition to a turbulent state of the non-ideal electric field spectrum (not shown here). However, at later times such sharp break is partially lost (see figure 1, bottom right panel), or hidden by other kind of fluctuations [10]). At this level, we cannot distinguish between the nature of the contributions to the small-scale spectrum as due to fluctuations continuously injected by fast reconnection or by coherent structures, but we claim that the fast turbulent reconnection mechanism is an essential ingredient for populating (or mediating the transfer of fluctuations to) the subproton-scale turbulence. Further evidence of the role of CSs reconnection is given by a comparison between the nonlinear cascade time at a given scale, $\tau_k \sim (k^3\mathcal{E}(k))^{-1/2}$, and the time needed to set up the subproton-scale spectrum. The former timescale is in agreement with the observed time needed for the formation of the spectrum up to $k_\perp d_i \lesssim 2$, while being much

longer with respect to the time over which we do observe the rapid rise of the subproton part of the spectrum, $k_\perp d_i \gtrsim 2$, which exhibits a speed-up of its formation and actually sets up on a timescale compatible with that of the first fast reconnection processes (see section 3.2).

As a matter of fact, we can state that a fully-developed turbulent state extending beyond the inertial range involves fast reconnection processes since, as the MHD-like cascade goes on, strong CSs are always formed on scales $\lesssim d_i$ until reconnection is triggered. The current sheets can be seen as the typical lower end of the MHD turbulent cascade, before entering the kinetic regime. As soon as reconnection takes place, small-scale magnetic fluctuations at scales $\lesssim d_i$ are consequently generated. The non-ideal electric field, being directly related to these magnetic field (and density) fluctuations, simultaneously rises. At $k_\perp d_i > 1$, such non-ideal components are by far the dominant contribution to the electric field fluctuations and are related to magnetic field line breaking (which in our simulation is ultimately given by an 'effective resistivity'). Reconnection processes, in turn, convert part of the small-scale magnetic energy into kinetic energy, giving a feedback on the ideal part of the electric field at small scales. If the energy is continuously injected at large scales, a quasi-steady turbulent state can be achieved only if a balance between the magnetic, velocity and electric fluctuations is reached. In a scenario where large-scale turbulent motions continuously generate current sheets, the non-ideal electric field and magnetic reconnection processes are therefore the perfect small-scale mediators for such a balance. In this regard, turbulence and magnetic reconnection can be seen as tightly entwined processes that feed on each other, in agreement with earlier results for what concerns the role of turbulence on reconnection and multiple X-point formation but limited to the MHD regime [55].

We conjecture that the above picture holds regardless of the electron physics at the reconnecting micro-layer with respect to other non-physical diffusion mechanisms, provided that the scale separation between d_i and the reconnection scale is large enough. The only requirement is the occurrence of 'fast enough' magnetic reconnection processes taking place on timescales shorter than (or comparable to) those of wave mode interactions.

3.2. Reconnection in a turbulent environment

In the following we focus on the problem of the CS destabilization via secondary instabilities, first of all magnetic reconnection, within a large-scale turbulent environment. The CS destabilization is a well known phenomenon, in particular in the context of plasma turbulence fed by any external energetic source as, for example, shear flow instabilities, able to build up elongated CS that typically shrink in the transverse direction up to the 'reconnection scale' eventually leading to the formation of (chain of) coherent structures [33, 34]. No doubt, the electron physics is needed to account for the correct mechanism underlying the development of reconnection. However, provided that the reconnection timescale is fast enough for reconnection to occur before the system itself destroys such conditions [56–58], the generation of magnetic islands and the related dynamics should proceed likewise even within the framework of a hybrid model. Here fast enough means also that the process is able to feed and set up the subproton spectrum faster with respect to the characteristic cascade time needed to extend the MHD inertial spectrum below the ion gyroradius, where wave modes and turbulent fluctuations are indeed found to be significantly different with respect to those in the MHD range. Our aim here is to discuss in detail the dynamics, in the physical space, induced by the energy cascading from the MHD inertial spectrum to the subproton scales. Indeed, the formation and disruption of relatively short CSs (of typical length L of the order of tens of d_i) is a key process for setting up a stationary spectrum below the ion kinetic scales. Therefore, in the following, even if the main features observed in our simulations are somewhat known from reconnection-focused studies, we shall illustrate the dynamics associated to the CS disruption in a turbulent environment.

At the end of the simulation, many (almost all) CSs will be destabilized leading to the formation of a large number of magnetic coherent structures, some of them in the form of magnetic islands, embedded in a isotropic sea of relatively large-amplitude perturbations. However, in the fully-developed turbulent stage, a clear analysis of single CS destabilization would be difficult and less accurate. Therefore, for the sake of clarity, we focus our analysis around the end of the first phase, i.e., when one of the first CSs just formed is destabilized, allowing us to unambiguously identify the physical processes underlying the CS disruption. This particular case has to be considered as our 'rosetta stone', since the same qualitative behavior is also observed during the subsequent CSs destabilization, but when the surrounding environment is much more perturbed that would make the analysis much less clear.

In figure 4 we show the shaded iso-contours of the out-of-plane current density, $j_z(x, y)$, at four different times, $t\Omega_{ci} = 132, 145, 160, 180$, respectively. These times span from the first magnetic reconnection event in the upper left CS (located in the region $0 \lesssim x/d_i \lesssim 30$ and $40 \lesssim y/d_i \lesssim 45$, upper left panel of figure 4) until its complete disruption through multiple events, leading to the formation of a chain of magnetic structures (lower right panel of figure 4). Hereafter, we will refer to that CS as CS1, for shortness. Note that, when a fully-developed turbulent state is reached, almost no trace of CS1 is left, the resulting coherent structures having been advected away from their formation sites and many new CSs having been formed due to large-scale motions (cf

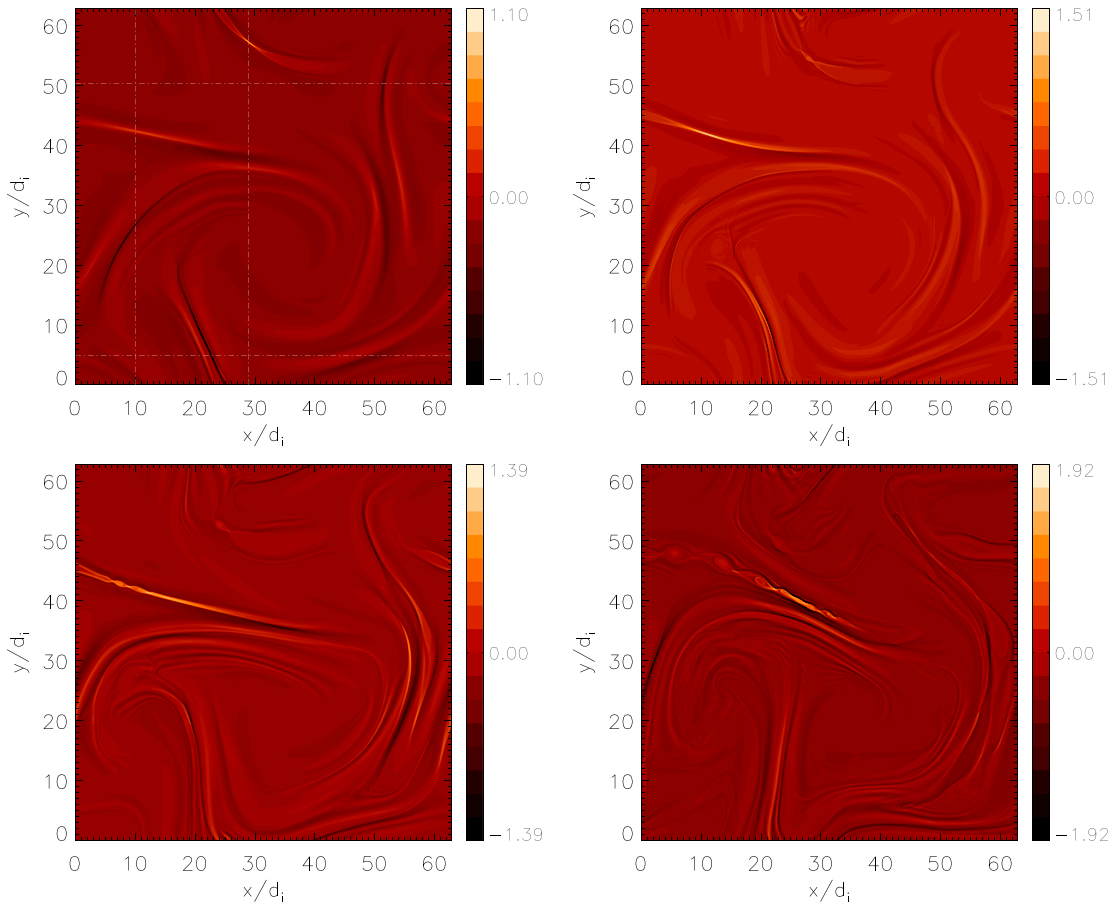

Figure 4. Iso-contours of the out-of-plane current density, j_z, at $t\Omega_{ci} = 132$, 145, 160, and 180, upper left, upper right, lower left and lower right panel, respectively. In the upper left panel, dash-dotted straight lines represent the cuts along which magnetic profiles are plotted in figure 5.

the left panels of figure 1). In the upper left frame of figure 4, we observe the presence of several CSs all over the simulation domain resulting, after more than 100 ion times, from the large-scale MHD dynamics driven by the external forcing. As already mentioned, the width of these structures has shrink down to the ion scale, $\delta_{cs} \sim d_i$, which is much smaller than the scale at which the forcing injects the energy, $30 \lesssim L_F/d_i \lesssim 60$. This means that the formation of the CSs is not a direct feature of our particular choice of the external forcing (we remind the reader that these structures are indeed formed also when a purely incompressible forcing is applied), but they rather develop as a typical feature of the turbulent cascade from the MHD scales [51]. At first, the CS1 becomes unstable and magnetic reconnection events are triggered until its complete disruption, eventually leading to a series of magnetic islands (see figure 4). The other CSs will share the same fate of CS1, one after each other (not shown here). The continuous formation and disruption of CSs is an ubiquitously repeated process happening throughout the fully-developed turbulent phase.

The disruption of a CS into a chain of magnetic structures can be triggered by the so-called plasmoid instability [59, 60], observed in general in the presence of an *ab initio* prepared CS which is several hundred times longer than its width [62]. Here the typical length L of the CSs is of the order of a few tens of its width, $a \sim d_i$, which, even for very large Lundquist numbers [61] seems to be too small, $L/a \ll 300$, to account for the so-called Hall reconnection triggered by plasmoids, as discussed in [63] (where they adopt a Hall–MHD framework and start from a straight current sheet as the initial equilibrium). In our case, although the dynamics and the parameters range might be similar to the one driven by the plasmoid instability, we reach an aspect ratio L/a much smaller than the expected one. This could be due to the fact that fast reconnection already proceeds on ideal timescales before a very large L/a value can be dynamically reached [64–66]. Moreover, it is worth stressing that the parameter space illustrated in figure 1 of [63] is mainly limited to a qualitative validity, as stated by the authors, since in large part still unexplored.

In our simulations the magnetic island generation always arises spontaneously, without any *ad hoc* initial conditions and/or without imposing any particular boundary condition that could directly drive or influence such mechanism, as in general done in reconnection-oriented studies where the simulation is initialized using a Harris-sheet-like configuration. In our case we leave the system to 'naturally' develop and meet the conditions

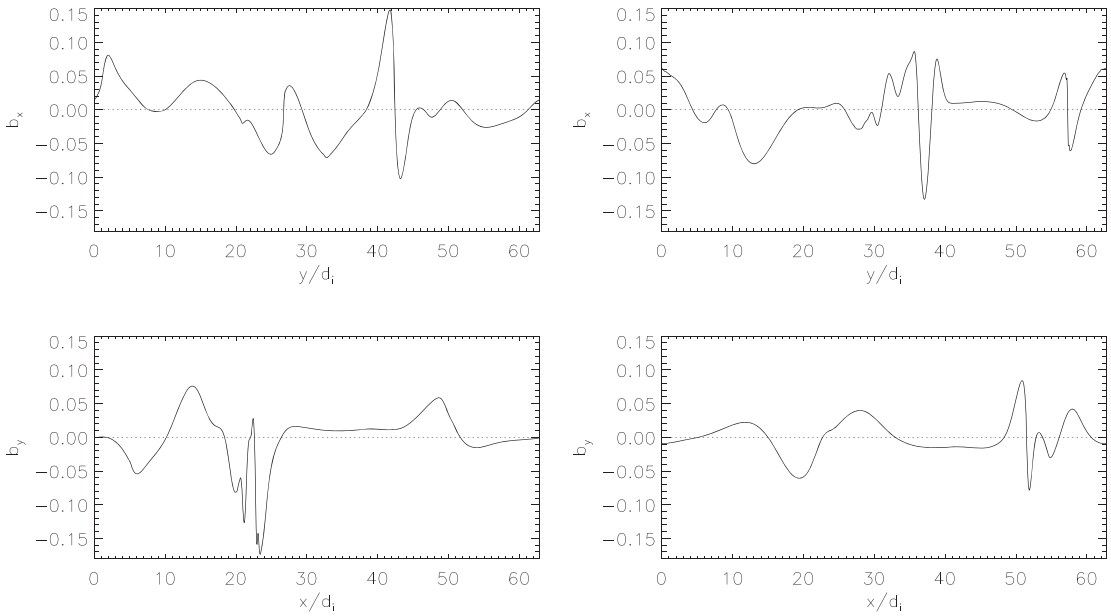

Figure 5. Horizontal and transverse cuts of the simulation plane at $t\Omega_{ci} = 132$ as shown in the top left frame of figure 4. The picture shows the following magnetic profiles: $b_x(y)$ at $x = 10,\ 29$, top left and right, respectively, and $b_y(x)$ at $y = 5,\ 50$, bottom left and right, respectively.

for single/multiple reconnection events to occur; on the other hand, such an approach has all the analysis-related difficulties of developing these processes in an 'uncontrolled' way. Here, for naturally we mean that no CSs are imposed at $t = 0$, any magnetic shear at the initial time being very weak ($|\delta\mathbf{b}(t = 0)| \lesssim 10^{-2}$) and on very large-scale lengths, $L > 10\ d_i$. In general, as our simulations go on, we see that the CSs form either as a single CS or as double (or multiple) CSs, with opposite signs of j_z and next to each other. Correspondingly, the magnetic field is characterized by one, two or more reversal when crossing those CSs. This behavior of the magnetic field is shown in figure 5, where we plot the magnetic field profiles taken along the dash-dotted line shown in the upper left frame of figure 4. These are, namely, $b_x(y)$ at $x = 10,\ 29$, upper left and right panel, respectively, and $b_y(x)$ at $y = 5,\ 50$, lower left and right panel, respectively.

The upper left frame of figure 5 shows the magnetic inversion at $y \simeq 42.5$ characterizing the CS1, which occurs on a length scale of order of $\sim d_i$. Other signatures of magnetic inversion, either single or multiple, can be seen in all the frames shown in figure 5, still on a d_i length scale. At that scale, the system (and its turbulent cascade) has left the MHD domain and enters a kinetic regime, eventually reaching a fully-developed turbulence. As discussed in the previous sections, the transition to turbulence occurs as soon as the instabilities developing at the CSs take over: at $t\Omega_{ci} = 180$, corresponding to the last time shown in figure 4, the turbulent transition process is in progress, the energy spectra of the different fields having not completely reached yet a fully stationary state for $kd_i \gg 1$ (see figure 1 and related text). We remind the reader that the saturated phase begins at about $t\Omega_{ci} \sim 150$, whereas we consider the quasi-steady turbulent state for $t\Omega_{ci} \gtrsim 200$, so the following analysis on CS1 belongs to the transition phase. The fast reconnection events involving CS1 as well as many different CSs at further times represent the main ingredient marking such transition and characterizing the successive fully-developed turbulent state.

Before focusing on CS1 reconnection events, we note that the first reconnection involves the CS located at the top of figure 4, upper left panel, where we observe a magnetic inversion with a very steep gradient (see the upper right plot of figure 5, at about $y \sim 57$) leading to the formation of a single magnetic island, as shown in the upper right panel of figure 4 at $x \sim 27$, $y \sim 54$. However, the CS is very short as compared to the others and presents a non-negligible curvature; as a result, right after the formation of the magnetic island the CS opens up, preventing any further reconnection event and leaving that particular magnetic structure as isolated. On the other hand, the much longer and almost straight CS1 exhibits the formation of two consecutive magnetic islands (lower left frame of figure 4 at $x \simeq 8$, $y \simeq 43$) and, remaining almost unchanged on both sides, it allows for reconnection to continue to occur eventually leading to the formation of a series ('chain') of magnetic structures, as shown in the lower right frame of figure 4.

Let us now address the full destabilization and disruption dynamics of CS1. We first look at the signatures of magnetic reconnection present in the two magnetic islands at $t\Omega_{ci} = 165$ (lower left frame of figure 4 at $x \simeq 8$, $y \simeq 43$). In figure 6 we show a zoom on these two magnetic structures at $t\Omega_{ci} = 165$ by drawing the shaded iso-

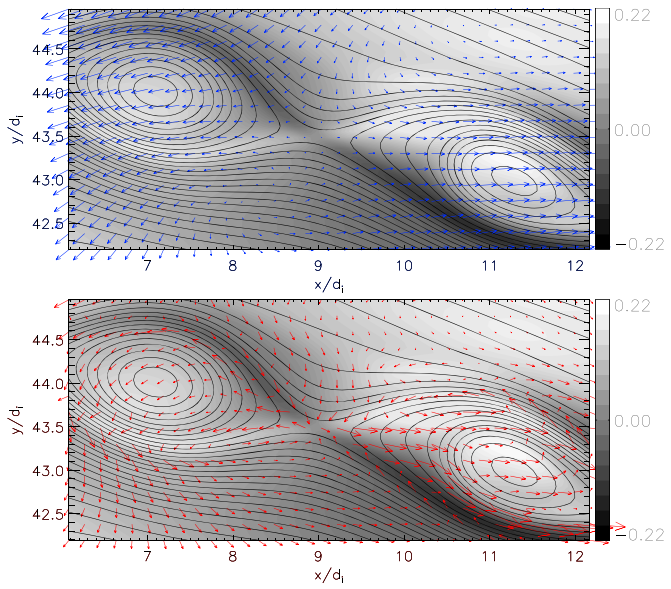

Figure 6. Shaded iso-contours of the density fluctuations, δn, and in-plane magnetic field lines (solid lines) at $t\Omega_{ci} = 165$. The blue and red arrows represent the ion and the electron flow in the X-point reference frame (top and bottom panel, respectively).

contours of the density fluctuations. The dark continuous lines represent the in-plane magnetic field lines in the $(x,\ y)$ plane, and the arrows show the ion (blue arrows) and the electron (red arrows) in-plane flow, top and bottom frame, respectively. These flows have been computed in the X-point reference frame. First of all, we observe the so-called Hall quadrupole around the X-point, an unambigous signature that fast magnetic reconnection was at play. The same quadrupole, but of opposite polarity, is observed on the out-of-plane magnetic field, δb_z, the so-called Hall field. The density and the magnetic quadrupole have opposite polarity because of pressure balance arguments: in order to have mechanical equilibrium, the perpendicular total pressure has to be constant across the structure, $P_{\perp,\mathrm{tot}} = B^2/2 + (\Pi_{xx} + \Pi_{yy})/2 + P_e \simeq$ const., where $P_e \propto n$ (isothermal electrons). Such balance has been verified numerically in our simulations (not shown here). Other reconnection signatures can be seen by analyzing the in-flows and out-flows at the reconnection site. By in- and out-flow here we mean the velocity field when crossing the X-point in the x and y-direction, i.e. $u_{a,y}(x_p,\ y)$ and $u_{a,x}(x,\ y_p)$ where $(x_p,\ y_p)$ corresponds to the X-point of figure 6 and $a = p,\ e$ indicates the species. Note that we are assuming the x-axis as nearly parallel to CS1 (and, later on, with the line connecting the two island centers). We find that the in-plane electron flow is responsible for the quadrupole lobes, so that the corresponding currents are the only ones associated with the δb_z fluctuations, while the in-plane ion flow varies smoothly and it is completely de-correlated from the quadrupole structure. At the X-point, the electron in-flow reaches a maximum value of the order $u_{e,\perp}^{\mathrm{inflow}} \sim 0.1\ v_A$, whereas the corresponding out-flow is even stronger, of order $\sim 0.2 \div 0.3\ v_A$. These flows are slightly 'left-right asymmetric' with respect to the X-point since the reconnection process is taking place in a non-uniform background, as outlined also by the slightly asymmetric shape of the magnetic islands in figure 6.

In figure 7 we show the x-component of the electron velocity, $u_{e,x}$, when reconnection is starting, top left frame, and when the islands are well formed, top right frame. This component nearly represents the electron out-flow from the X-point. Correspondingly, the profiles of several quantities along the transverse y-direction, and crossing the X-point, are shown in the bottom frames (see caption). Initially, top left frames, we observe the formation of a relatively intense out-flow from the reconnection region around $x \simeq 11.5$, well aligned with CS1. This flow increases as reconnection goes on (see color codes for $u_{e,x}$ in the top frames). Once the magnetic islands are formed, top right frame, the electron flow partially circulates inside the inner part of the island and then, far from the island, continues straight on along CS1 for $x \gtrsim 14$. Focusing on the in-flow velocities profiles across the X-point, $u_{i,y}(y)$ and $u_{e,y}(y)$ exhibit an asymmetric behavior both in shape as in peak values (see figure 7 bottom frames). Furthermore, we see the scale separation of the two species in the so-called 'diffusion region' which turns out to be of about $\delta_e < 1 d_i$ for the electrons (here, since $m_e = 0$, that thickness is set by an effective grid resistivity), and about $\delta_i \sim 3\ d_i$ for the ions. The same qualitative features are observed also in the out-flows (not shown here).

By inspecting the magnetic profiles one notes that their gradient has increased during X-point formation and that it remains very stiff even when the islands are well formed. Unfortunately, the variation of the magnetic field gradient and the fact that the CS is differentially moving advected by the large-scale velocity field, does not allow

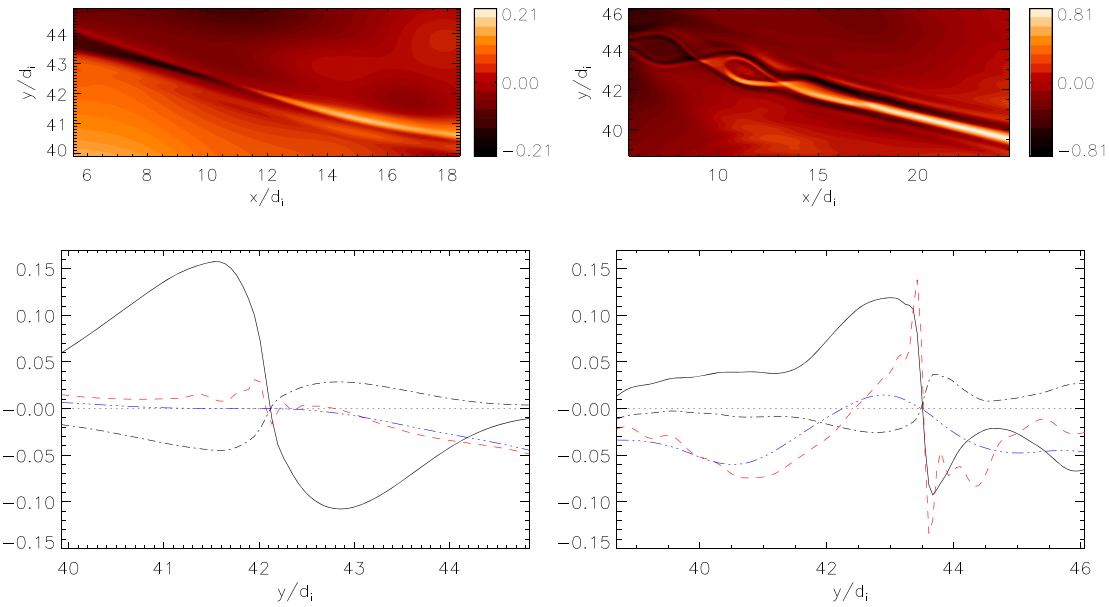

Figure 7. Top frames: the shaded iso-contours of the x-component of the electron velocity, $u_{e,x}$, at $t\Omega_{ci} = 137,\ 165$, respectively. Note that the domains are slightly different in the two cases. Bottom frames: corresponding y-profiles, at $x = 11.5$ and $x = 8.9$, respectively, of b_x (black solid line), b_y (dotted-dashed line), $u_{e,y}$ (red dashed line), and $u_{i,y}$ (blue dashed-three-dotted line).

us to calculate a growth rate. However, by considering that the magnetic islands do form in about 30 ion times, we can estimate a growth rate of the order of 0.1 (ion units).

The CS-aligned electron flow emerging at the sides of the islands (i.e. for $x \gtrsim 14$ in figure 7) forms a jet-like structure where the electron velocity reaches nearly the Alfvén speed, $u_e \sim 0.8\ v_A$. Correspondingly, two less-intense flows in the opposite direction, with about $u_e \sim 0.2\ v_A$, are observed at the jet sides (since they are essentially given by j/n, we can talk about 'returning currents'). This would be a typical configuration where kinetic instabilities, such as the two-stream or current filamentation instability would develop (assuming, by including kinetic electrons, a return current more superposed to the initial one); in our hybrid model the transition to kinetic electron micro-instabilities cannot be observed. Most important, the velocity shears associated to the central and to the returning currents are located on the two sides of the magnetic field gradient, which is in turn located at the center of the CS1 (corresponding to the center of the outgoing electron flow). Such a shift of the velocity shear with respect to the magnetic shear has a consequence on reconnection and on secondary instabilities that can possibly develop. Indeed, if the magnetic and velocity shear would be superposed, the latter would possibly have a stabilizing effect on reconnection (see [67] and references therein), while in our case the separation between the magnetic and velocity shears makes the system potentially unstable to a Kelvin–Helmholtz (KH)-like instability at the edge of the reconnection layer. As a result, the velocity shears might force reconnection. We have indeed verified that, due to the magnetic tension, the KH is inhibited and therefore cannot develop in the form of fully rolled-up vortices. Nevertheless, we conjecture that even partially inhibited, the slowly-growing KH-like perturbations can force reconnection to develop.

We now discuss more in detail the jet formation process and development. First of all, in about ten ion times it becomes quite extended, much longer than the characteristic extension length of the two magnetic islands. This is shown in figure 8 and in figure 9 where we draw the x-component of the current, j_x, at progressive times (note that the space domain in figure 9 is a bit larger than in figure 8). Starting at $t = 137$ by the formation of the flow exiting from the reconnection region along the CS, first frame of figure 8, a jet-like structure progressively forms and extends becoming more and more intense (second frame). The jet formation ends more or less when the two magnetic islands saturates, $t = 160$, first bottom frame of figure 8 and it is characterized, as already discussed, by a central electron flow along the positive x-direction (corresponding to a negative j_x current as shown by the blue channel in figure 9) and by two return channels (the yellow ones in figure 9) on both sides with respect to the central one. This structure lying in the $(x,\ y)$ plane can be considered as a CS now along the x-direction, but since our simulations are limited to the $(x,\ y)$ plane, i.e. $\partial/\partial z = 0$, it cannot give rise to the reconnection that would now develop in the $(y,\ z)$ plane. Nevertheless, from the point of view of the transition to turbulence, the electron channel becomes very rapidly unstable by starting bending and draping, see the first frame of figure 9 at $t = 178$. Indeed, reconnection starts but this time is evolving much more rapidly than for the formation of the first two magnetic islands discussed before. In particular, in about less than 10 ion times, the channel has evolved into a complex chain of magnetic islands as shown by the second frame of figure 9 at

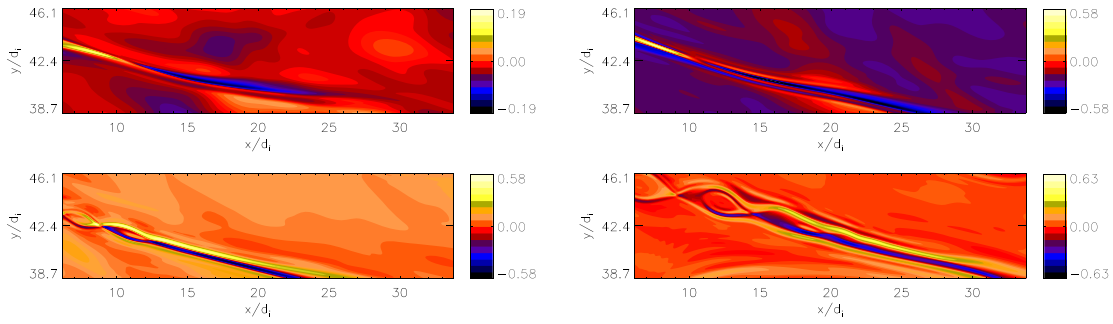

Figure 8. Shaded iso-contours of the x-component of the current density, j_x, at $t\Omega_{ci} = 137,\ 150,\ 160,\ 170$, respectively.

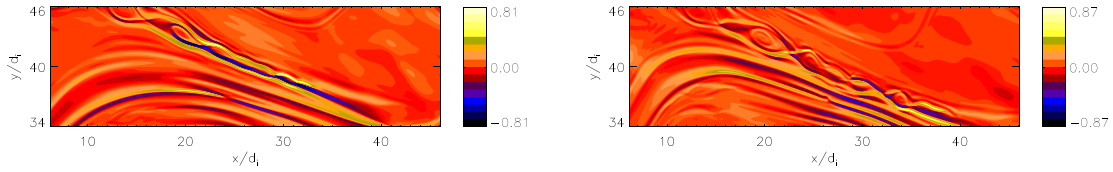

Figure 9. Same as figure 8 at $t = 178,\ 185$, respectively, but for a larger space domain.

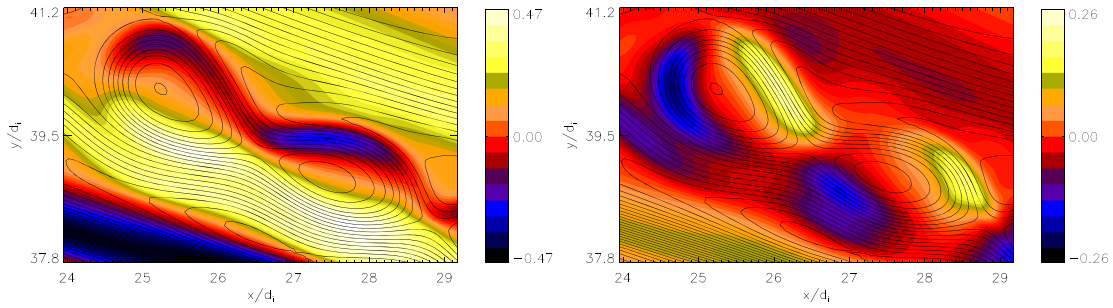

Figure 10. The shaded iso-contours of δb_x and of δb_y, first and second frame, respectively. The continuous lines correspond to the magnetic field lines in the $(x,\ y)$ plane.

$t = 185$. We underline that all the magnetic islands have been generated into the channel more or less during the same time period, instead of a cascade-like process where each island triggers the next island along the channel. In other words, once the jet-structure along the CS1 has been formed, reconnection starts to generate the islands more or less simultaneously. We argue that the velocity shear at the edge of the magnetic field reversal, by possibly introducing KH-like magnetic fluctuations or by dynamically squeezing/elongating the CS (i.e., lowering the ratio a/L), could be responsible for accelerating the development of reconnection [65, 66]. Transition to fast magnetic reconnection is a fundamental aspect for the understanding of its connection to the turbulent cascade across the ion break: the turbulent cascade proceeds in the standard way, setting up the $-5/3$ spectrum accordingly to the nonlinear timescale up to $k_\perp d_i \lesssim 2$ where magnetic reconnection starts to occur on very short timescales (about $t \sim 170$, cf figures 1, 8 and 9). Correspondingly, the small-scale spectrum rapidly rises to establish the same spectrum which is observed in the quasi-steady turbulent state, along with the characteristic ion break. The formation of the subproton-scale spectrum thus happens on timescales that are smaller than the standard nonlinear cascade time at $k_\perp d_i > 1$, but compatible with the short timescales on which fast magnetic reconnection proceeds (as it is boosted by the process described above).

Finally, we have selected two typical such structures in the domain $24 \leqslant x \leqslant 29$, $38 \leqslant y \leqslant 41$ at time $t = 230$, late enough to consider them as more or less stable coherent structures. These structures are shown in figure 10 where we draw the shaded iso-contours of δb_x and of δb_y, left and right frame, respectively, with the over-plotted the magnetic field lines in the $(x,\ y)$ plane. Both pictures are reminiscent of the so-called Alfvén vortex-like structure (see for instance [49] and references therein) even if the turbulent environment alters the symmetries of the analytical solutions.

4. Conclusions

We have presented an analysis of 2D-3V Vlasov-hybrid simulations of plasma turbulence fed by an external, low-amplitude random forcing. The forcing acts at the largest scale lengths allowed by the simulation box, much larger than the ion kinetic scale, and allows the system to eventually reach a fully-developed quasi-steady turbulent state. An analysis concerning the observed turbulent spectra and their interpretation as a function of the plasma beta parameter have been recently reported in [41]. Here we have focused on the role and interplay of small-scale electromagnetic fluctuations and magnetic reconnection for the development of such turbulent state at $\beta = 1$.

We have shown that a spectrum close to a $-5/3$ power law sets up at large scales, $kd_i \lesssim 1$, according to the correspondent nonlinear cascade time. At the same time the system develops many current sheets randomly distributed over the simulation domain. However turbulence at smaller scales, below the ion kinetic scales, seems to be mediated by fast magnetic reconnection processes that quickly bring the system to a fully-developed turbulent state. Such transition has been shown to be related to the destabilization via magnetic reconnection of the current sheets and to the corresponding formation of d_i-scale coherent structures and rise of small-scale non-ideal electric fields at $k_\perp d_i > 1$. In particular, it has been shown that the nature of the non-ideal electric field undergoes a rapid change which is related to the transition to fully-developed turbulence induced by fast reconnection processes: such electric fluctuations pass from being dominated by the gradients at the front of the large-scale vortical motions, to being completely localized within current sheets and magnetic structures whose sizes (or width) are of the order of d_i, and only at that point a stationary small-scale turbulent spectrum is formed. Current sheets, continuously generated by large-scale turbulent motions, are thus disrupted by fast reconnection on timescales which are smaller than the nonlinear cascade time at the reconnecting scales, allowing the system to rapidly reach a fully-developed quasi-steady turbulent state where a balance between the magnetic, velocity and electric fluctuations is achieved. In fact, a closer analysis of the current sheet destabilization mechanism during such transition to fully-developed turbulence, allowed us to show the possibility of creating very rapidly a large number of coherent structures by a speed-up of the reconnection process. These structures rapidly fill the spectrum around d_i-scales and excite fluctuations at the subproton scales which then cascade towards smaller and smaller scales. We have therefore identified the fast magnetic reconnection processes as the preferred (or concurrent) mediators for the cascade at small-scales, thus picturing turbulence and magnetic reconnection as tightly entwined self-regulating processes that feed on each other. In our opinion, such a mechanism is crucial for developing a self-regulated turbulent state across and below the ion kinetic scale lengths.

In summary, the transition between the inertial and the subproton-scale spectrum is mediated by the formation of coherent structures and by the associated small-scale non-ideal electric field emerging from the destabilization of 'large-scale' current sheets by fast magnetic reconnection. The coherent structures formation process, accelerated by the presence of strong jets, is rapid enough to be competitive with wave mode interactions leading to the formation of a fully-developed turbulent spectrum across the so-called ion break. We thus propose that the formation of coherent structures by fast reconnection processes can be the crucial mechanism that continue the nonlinear cascade across the ion break. We conjecture that the above picture holds regardless of the electron physics at the reconnecting micro-layer with respect to other non-physical diffusion mechanisms, provided that the scale separation between d_i and the reconnection scale is large enough. The only requirement is the occurrence of 'fast enough' magnetic reconnection events developing on a timescale shorter than (or comparable to) those of the wave mode interactions.

Acknowledgments

We gratefully acknowledge F Pegoraro, L Franci and A Tenerani for useful discussions. The authors thank Dr C Cavazzoni (CINECA, Italy) for his essential contribution to code parallelization and performance, and F Rincon for the implementation of the external forcing in the HVM code. We acknowledge the anonymous referee for the useful comments that helped improve the presentation and the discussion of the results. The simulations presented in this work were carried out using the Hydra supercomputer at the Max Planck Computing and Data Facility (MPCDF), Garching, Germany. We also acknowledge CINECA for the access to the Galileo supercomputer where a number of tests on the external forcing have been performed under ISCRA allocation projects (grants HP10CGW8SW and HP10C04BTP).

References

[1] Bruno R and Carbone V 2013 *Living Rev. Solar Phys.* **10** 2

[2] Bale S D, Kellogg P J, Mozer F S, Horbury T S and Reme H 2005 *Phys. Rev. Lett.* **94** 215002
[3] Alexandrova O, Carbone V, Veltri P and Sorriso-Valvo L 2008 *Astrophys. J.* **674** 1153
[4] Sahraoui F, Goldstein M L, Robert P and Khotyaintsev Yu V 2009 *Phys. Rev. Lett.* **102** 231102
[5] Alexandrova O, Saur J, Lacombe C, Mangeney A, Mitchell J, Schwartz S J and Robert P 2009 *Phys. Rev. Lett.* **103** 165003
[6] Chen C H K, Horbury T S, Schekochihin A A, Wicks R T, Alexandrova O and Mitchell J 2010 *Phys. Rev. Lett.* **104** 255002
[7] Sahraoui F, Goldstein M L, Belmont G, Canu P and Rezeau L 2010 *Phys. Rev. Lett.* **105** 131101
[8] Matthaeus W H and Goldstein M L 1982 *J. Geophys. Res.* **87** 6011
[9] Bieber J W, Wanner W and Matthaeus W H 1996 *J. Geophys. Res.* **101** 2511
[10] Lion S, Alexandrova O and Zaslavsky A 2016 *Astrophys. J.* **824** 47
[11] Howes G G, Cowley S C, Dorland W, Hammett G W, Quataert E and Schekochihin A 2008 *J. Geophys. Res.* **113** A05103
[12] Schekochihin A A, Cowley S C, Dorland W, Hammett G W, Howes G G, Quataert E and Tatsuno T 2009 *Astrophys. J. Suppl. Series* **182** 310
[13] Boldyrev S and Perez J C 2012 *Astrophys. J. Lett.* **758** L44
[14] Boldyrev S, Horaites K, Xia Q and Perez J C 2013 *Astrophys. J.* **777** 41
[15] Stawicki O, Gary S P and Li H 2001 *J. Geophys. Res.* **106** 8273
[16] Galtier S and Bhattacharjee A 2003 *Phys. Plasmas* **10** 3065
[17] Matthaeus W H, Oughton O, Osman K T, Servidio S, Wan M, Gary S P, Shay M A, Valentini F, Roytershteyn V and Karimabadi H 2014 *Astrophys. J.* **790** 155
[18] Perri S, Goldstein M L, Dorelli J C and Sahraoui F 2012 *Phys. Rev. Lett.* **109** 191101
[19] Greco A, Perri S, Servidio S, Yordanova E and Veltri P 2016 *Astrophys. J. Lett.* **823** L39
[20] Ma Z W, Lee L C and Otto A 1995 *Geophys. Res. Lett.* **22** 1737
[21] Ma Z W and Lee L C 1999 *J. Geophys. Res.* **104** 10177
[22] Sturrock P A 1999 *Astrophys. J.* **521** 451
[23] Passot T and Sulem P-L 2015 *Astrophys. J. Lett.* **812** L37
[24] Boldyrev S, Chen C H K, Xia Q and Zhdankin V 2015 *Astrophys. J.* **806** 238
[25] Shaikh D 2009 *Mon. Not. R. Astron. Soc.* **395** 2292
[26] Shaikh D and Zank G P 2009 *Mon. Not. R. Astron. Soc.* **400** 1881
[27] Valentini F, Califano F and Veltri P 2010 *Phys. Rev. Lett.* **104** 205002
[28] Parashar T N, Servidio S, Breech B, Shay M A and Matthaeus W H 2010 *Phys. Plasmas* **17** 102304
[29] Parashar T N, Servidio S, Shay M A, Breech B and Matthaeus W H 2011 *Phys. Plasmas* **18** 092302
[30] Howes G G, Dorland W, Cowley S C, Hammett G W, Quataert E, Schekochihin A A and Tatsuno T 2008 *Phys. Rev. Lett.* **100** 065004
[31] Howes G G, TenBarge J M, Dorland W, Quataert E, Schekochihin A A, Numata R and Tatsuno T 2011 *Phys. Rev. Lett.* **107** 035004
[32] Servidio S, Valentini F, Califano F and Veltri P 2012 *Phys. Rev. Lett.* **108** 045001
[33] Wan M, Matthaeus W H, Karimabadi H, Roytershteyn V, Shay M, Wu P, Daughton W, Loring B and Chapman S C 2012 *Phys. Rev. Lett.* **109** 195001
[34] Karimabadi H *et al* 2013 *Phys. Plasmas* **20** 012303
[35] Servidio S, Osman K T, Valentini F, Perrone D, Califano F, Chapman S C, Matthaeus W H and Veltri P 2014 *Astrophys. J. Lett.* **781** L27
[36] Passot T, Henri P, Laveder D and Sulem P-L 2014 *Eur. Phys. J.* D **68** 207
[37] Franci L, Verdini A, Matteini L, Landi S and Hellinger P 2015 *Astrophys. J. Lett.* **804** L39
[38] Told D, Jenko F, TenBarge J M, Howes G G and Hammett G W 2015 *Phys. Rev. Lett.* **115** 025003
[39] Franci L, Landi S, Matteini L, Verdini A and Hellinger P 2015 *Astrophys. J. Lett.* **812** 21
[40] Sulem P-L, Passot T, Laveder D and Borgogno D 2016 *Astrophys. J.* **818** 66
[41] Cerri S S, Califano F, Jenko F, Told D and Rincon F 2014 *Astrophys. J. Lett.* **822** L12
[42] Mangeney A, Califano F and Cavazzoni C 2002 *J Comput Phys* **179** 495
[43] Valentini F, Califano F, Hellinger P and Mangeney A 2007 *J Comput Phys* **225** 753
[44] Karimabadi H, Roytershteyn V, Daughton W and Liu Y-H 2013 *Space Sci. Rev.* **178** 307
[45] Wan M, Matthaeus W H, Roytershteyn V, Parashar T N, Wu P and Karimabadi H 2016 *Phys. Plasmas* **23** 042307
[46] Li T C, Howes G G, Klein K G and TenBarge J M 2016 *Astrophys. J. Lett.* **832** L24
[47] Gary S P and Smith C W 2009 *J. Geophys. Res.* **114** A12105
[48] He J, Tu C, Marsch E and Yao S 2012 *Astrophys. J. Lett.* **745** L8
[49] Alexandrova O 2008 *Nonlin. Processes Geophys.* **15** 95
[50] Rossi C, Califano F, Retinò A, Sorriso-Valvo L, Henri P, Servidio S, Valentini F, Chasapis A and Rezeau L 2015 *Phys. Plasmas* **22** 122303
[51] Biskamp D 2003 *Magnetohydrodynamic Turbulence* (Cambridge: Cambridge University Press)
[52] Markovskii S A and Vasquez B J 2011 *Astrophys. J.* **739** 22
[53] Phan T D, Drake J F, Shay M A, Mozer F S and Eastwood J P 2007 *Phys. Rev. Lett.* **99** 255002
[54] Chasapis A, Retinò A, Sahraoui F, Vaivads A, Khotyaintsev Y V, Sundkvist D, Greco A, Sorriso-Valvo L and Canu P 2015 *Astrophys. J. Lett.* **804** L1
[55] Matthaeus W H and Lamkin S L 1986 *Phys. Fluids* **29** 2513
[56] Faganello M, Califano F and Pegoraro F 2008 *Phys. Rev. Lett.* **101** 175003
[57] Faganello M, Califano F and Pegoraro F 2008 *Phys. Rev. Lett.* **101** 105001
[58] Faganello M, Califano F and Pegoraro F 2009 *New J. Phys.* **11** 063008
[59] Loureiro N F, Schekochihin A A and Cowley S C 2007 *Phys. Plasmas* **14** 100703
[60] Daughton W and Roytershteyn V 2012 *Space Sci. Rev.* **172** 271
[61] Uzdensky D A, Loureiro N F and Schekochihin A A 2010 *Phys. Rev. Lett.* **105** 235002
[62] Markidis S, Henri P, Lapenta G, Divin A, Goldman M V, Newman D and Eriksson S 2012 *Nonlinear Processes Geophysics* **19** 145
[63] Huang Y-M, Bhattacharjee A and Sullivan B P 2011 *Phys. Plasmas* **18** 072109
[64] Pucci F and Velli M 2014 *Astrophys. J. Lett.* **780** L19
[65] Tenerani A, Velli M, Rappazzo A F and Pucci F 2015 *Astrophys. J. Lett.* **813** L32
[66] Del Sarto D, Pucci F, Tenerani A and Velli M 2016 *J. Geophys. Res. Space Physics* **121** 185
[67] Faganello M, Pegoraro F and Califano F 2010 *Phys. Plasmas* **17** 062102